

Thermally forced mesoscale atmospheric flow over complex terrain in Southern Italy

M. BALDI, M. COLACINO, G. A. DALU, E. PIERVITALI and Z. YE

Istituto di Fisica dell'Atmosfera (CNR) - Roma, Italy

(ricevuto il 16 Ottobre 1997; revisionato il 23 Marzo 1998; approvato il 6 Aprile 1998)

Summary. — In this paper we discuss some results concerning the analysis of the local atmospheric flow over the southern part of Italy, the Calabria peninsula, using a mesoscale numerical model. Our study is focused on two different but related topics: a detailed analysis of the meteorology and climate of the region based on a data collection, reported in Colacino *et al.*, *Elementi di Climatologia della Calabria*, edited by A. GUERRINI, *Collana P. S., Clima, Ambiente e Territorio nel Mezzogiorno* (CNR, Roma) 1997, pp. 218, and an analysis of the results based on the simulated flow produced using a mesoscale numerical model. The Colorado State University mesoscale numerical model has been applied to study several different climatic situations of particular interest for the region, as discussed in this paper. In particular, the effects on the circulation over the region, due to the variation of different physical parameters as large-scale flow intensity, vertical potential temperature gradients, soil moisture, have been studied, and the seasonal variability of the Thermally Forced Mesoscale Circulations (TFMCs) is presented. The results show that thermally forced mesoscale circulation in the region is rather complex, and more pronounced than in regions located at the same latitude. The cells are strongly supported by the presence of the two breeze systems (sea-land and mountain-valley), and their location, shape and intensity are affected by the intensity of the large-scale flow, while atmospheric stability and soil moisture have a weaker influence on the TFMC structure. This study of the dynamics and thermodynamics of the atmosphere in this region, and particularly the analysis of the wind field, is preliminary for other related topics of research as agrometeorology, wind energy exploitation, environmental impact assessment, and for research related to tourism.

PACS 92.60.Fm – Boundary layer structure and processes.

PACS 92.60.Gn – Winds and their effects.

1. – Introduction

The aim of this research is to study the general atmospheric circulation over the Calabria peninsula as a first step for further researches like diffusion and dispersion of

air pollutants on a local and/or regional scale, microclimate of smaller areas, and environmental impact assessment.

The atmospheric circulation of the region is strongly affected by the complex orography of the area, and local meteorological phenomena are superimposed to the synoptic scale circulation field, during the winter and the summer seasons. In particular, a strong sea breeze circulation and an upslope flow circulation are the two main phenomena occurring in the presence of calm or near calm synoptic situation and clear-sky conditions, all the year around. However, frequency is higher during summer, as well as the formation of convective clouds associated to the thermally forced mesoscale circulation (TFMC) resulting in a thermally induced upslope flow supported by the sea breeze during the diurnal hours.

The convection phenomenon initially triggered in the presence of calm or near calm synoptic flow is due to the effects of thermally forced mesoscale flows. Some research studies in US pointed out that out of a total of 482 significant rainstorms over the United States East of 109° W identified during the summers of 1982 and 1983, 52% could be attributed to mesoscale forcing.

Therefore, mesoscale circulation can play a fundamental role in determining the location and strength of cumulus convection in regions where differences in both surface heating and topography are as intense as in Calabria.

In order to analyze the effects produced by the local topography, the simulations have been performed using the mesoscale numerical model RAMS (Regional Atmospheric Modeling System) of the Colorado State University [1], since it is a powerful tool to describe the circulation over complex terrain [2].

In the following sections we discuss results of the numerical simulations, and in particular we discuss the seasonal variation of the TFMCs under calm and near calm conditions, and describe the impact of physical parameters like synoptic flow intensity, thermal stability of the atmosphere, available soil moisture, on the structure and evolution of TFMCs.

2. – General geomorphology and climate of the region

The Calabria peninsula, located in the southern part of the Italian peninsula, ranges between 38° and 40° latitude North, and between 16° and 17° 15' longitude East, and it is surrounded on three sides by the Mediterranean Sea (Thyrrhenian Sea on the West side, and the Ionian Sea South and East). The topography, shown in fig. 1, is characterized by the presence of the Southern Apennines range which runs in the direction North-South: Catena Costiera, La Sila, Le Serre, Aspromonte. The Catena Costiera is connected to the Central Apennines through the Scalone Pass (745 m a.s.l.). Two major valleys are located between the Catena Costiera and La Sila: Crati and Savuto. The highest mountain in La Sila range is Botte Donato (1929 m a.s.l.).

Soglia di Marcellinara, the gap between La Sila and Serre Ranges, represents the narrower point of the region in the direction East-West. The two ranges of Serre and Aspromonte are separated by the Mercante Pass and the peaks are Pecoraro in the Serre (1420 m a.s.l.) and Cocuzza (1956 m a.s.l.).

Three relatively great flat areas extending toward the sea, Sibari Plain in the East, on the Ionian coast, Lamezia and Gioia Tauro in the West, towards the Tyrrhenian sea, are the most populated and industrialized areas of the Region.

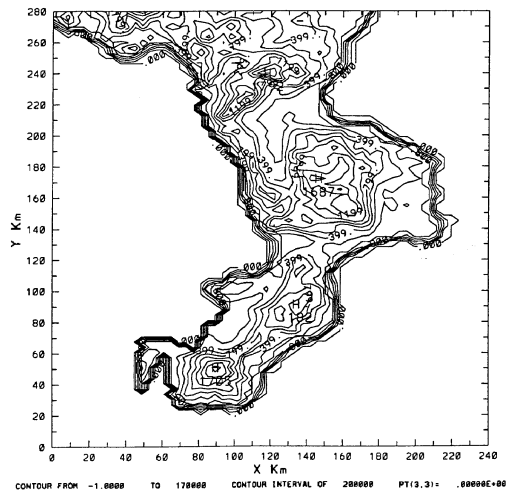


Fig. 1. – Orography of the Calabria Region.

The climate of the region is mainly influenced by the general Mediterranean climate; however, a local climate, induced by local phenomena, is superimposed to the synoptic situation, and several different microclimates characterize different areas of the region.

The Mediterranean climate is characterized by two different seasonal patterns: a cold season (November-April) and a warm season (June-September), while the two transient seasons are very short and not well defined [3,4]. This seasonal pattern is also evident in the Calabria climate, characterized by dry, sunny, and warm summers and wet, rainy, and mild winters.

Actually, the mean minimum temperature value in the Calabria region is about 6°C in winter, while the mean maximum is 30°C during summer. The topography of the region strongly influences the mean temperature field, and the vertical temperature gradient ($-0.63^{\circ}/100\text{ m}$) is very similar to the adiabatic case [5]. The relative humidity ranges between 70% and 90% during winter, and between 55% and 70% during summer, with a maximum of precipitation registered in the mountain stations (1430 mm/year), and a minimum along the coast (530 mm/year at the Reggio Calabria station). The wind maps present more persistent winds along the coast, with sea breeze circulation more effective in summer; however, the strong winds may occur in the interior and during the winter season.

3. – The numerical model

For the simulations, we have used the numerical model RAMS developed at the Colorado State University in its simplified hydrostatic and incompressible version, even though in its 3D and nonlinear version, in order to reduce computing time. RAMS [1] is a quite complex model, resulting from the merging of different numerical

TABLE I. – Simulations of several synoptic situations relative to different periods of the year, with different soil moisture conditions, atmospheric stability, synoptic wind.

Case	Synoptic flow intensity		Simulated day	Soil moisture (M)	Atmospheric stability (ϑ vertical gradient) (K/km)
	u_g (m/s)	v_g (m/s)			
1	0.0	0.5	Jan. 16	0.05	2.0
2	0.0	0.5	Jul. 16	0.05	2.0
3	0.0	0.5	Oct. 16	0.05	2.0
4	0.0	0.5	Jul. 16	0.2	2.0
5	0.0	0.5	Jul. 16	0.4	2.0
6	0.0	0.5	Jul. 16	1.0	2.0
7	0.0	0.5	Jul. 16	0.05	10.0
8	7.0	0.0	Jul. 16	0.05	2.0
9	10.0	0.0	Jul. 16	0.05	2.0
10	14.0	0.0	Jul. 16	0.05	2.0

codes previously developed by different research groups [6-8]. It also represents a great tool for air quality modeling, since its meteorological field output can be conveniently used as an input to regional and mesoscale models for air pollution [9-12].

The local complexity of the terrain is introduced by making use of a proper system of coordinates, the so-called terrain-following coordinates.

In this paper we present general results for the entire region, without going into the details of microscale phenomena and without using the full capabilities of the model, *i.e.* without using the nested-grids configuration, which can facilitate the detailed study of the dynamic and thermodynamic fields at different spatial scales, and of the microclimate of smaller areas of the Calabria peninsula, but it requires more computing time, so it can be used as a further development of this study.

Values of physical parameters like albedo, surface temperature, surface wind, etc., derived from the analysis of meteorological data [5], have been introduced as an input to the model. The initial synoptic wind field is assumed homogeneous over the entire region, assuming that it does not vary during the simulation itself, *i.e.* in this case, even if the dynamic fields are not re-adjusted to the new “true” values, however, the dynamic fields change in accordance to the fluxes in the lower layers, as computed by the model itself.

A detailed description of the Planetary Boundary Layer is introduced in the model [13], based on the balance between different radiation terms in the energy equation, as well as of the Convective Boundary Layer (CBL), using Deardorff's formulation for the heat balance and the diffusion equations for the latent and sensible heat introduced in the lower layers.

A pre-run of the model, assuring that the meteorological fields are almost in balance with the lower boundary drag due to the topography and to surface roughness, is necessary in order to infer to the atmosphere the appropriate baroclinicity corresponding to the observed synoptic shear.

Several synoptic situations, relative to different periods of the year (*i.e.* with different solar radiation) with different values of soil moisture conditions, atmospheric stability, synoptic wind, have been simulated, as summarized in table I.

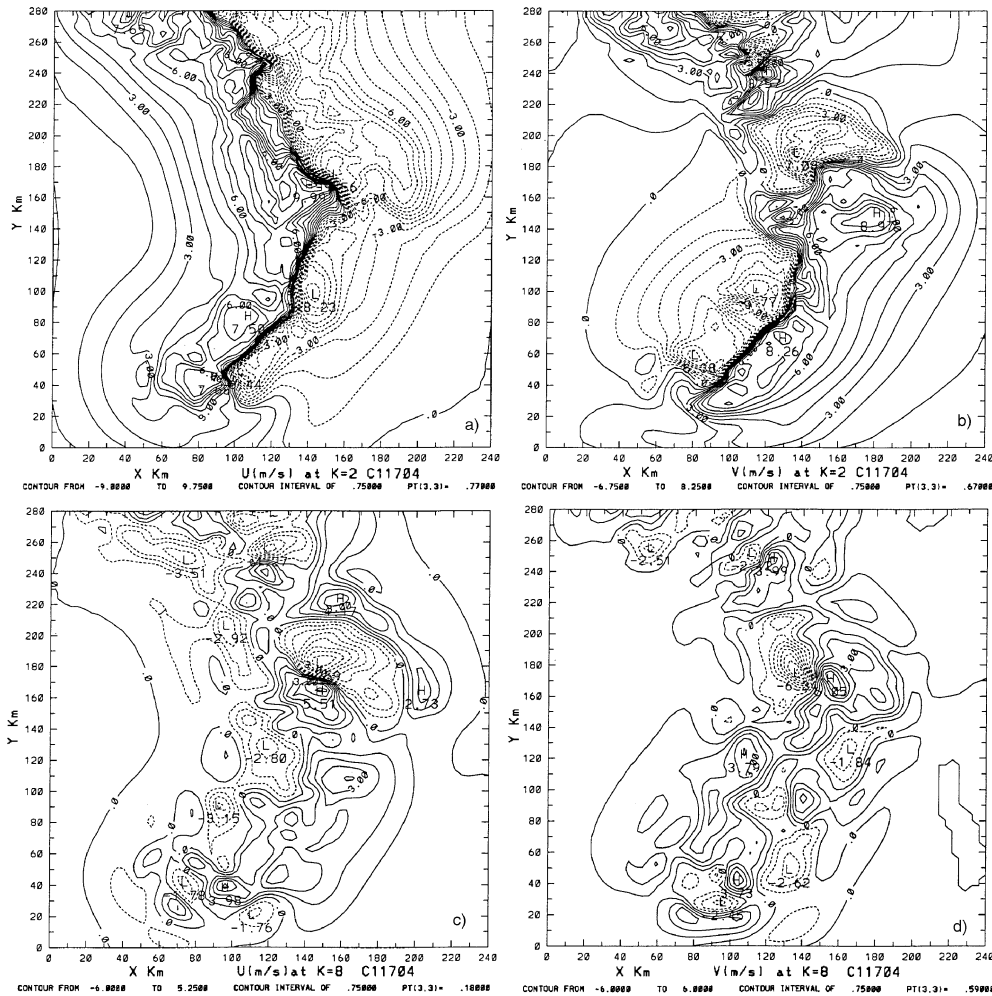


Fig. 2. - Summer case. Synoptic wind field = ($U_g = 0$; $V_g = 0.5$ m/s), soil moisture = 0.05, conductivity = 3.9 cm/s, density = 1.45 kg/m³, specific heat = 0.35 cal/(cm³ K), surface temperature = 288 K, atmospheric stability = 2 K/km. a) U -component of wind field at $z = 100$ m; b) V -component of wind field at $z = 100$ m; c) U -component of wind field at $z = 1600$ m; d) V -component of wind field at $z = 1600$ m.

4. - Modeling results

The vertical convection associated with thermally induced convergence represents a particularly intense phenomenon in the Calabria region during the summer season; however, it can occur also during the winter season in the presence of very weak synoptic circulation.

Due to the steepness of the region and to its narrow dimension in the E-W direction, the TFMC is the result of the interaction of two phenomena: the sea breeze circulation superimposed to the upslope winds, induced by the mountains.

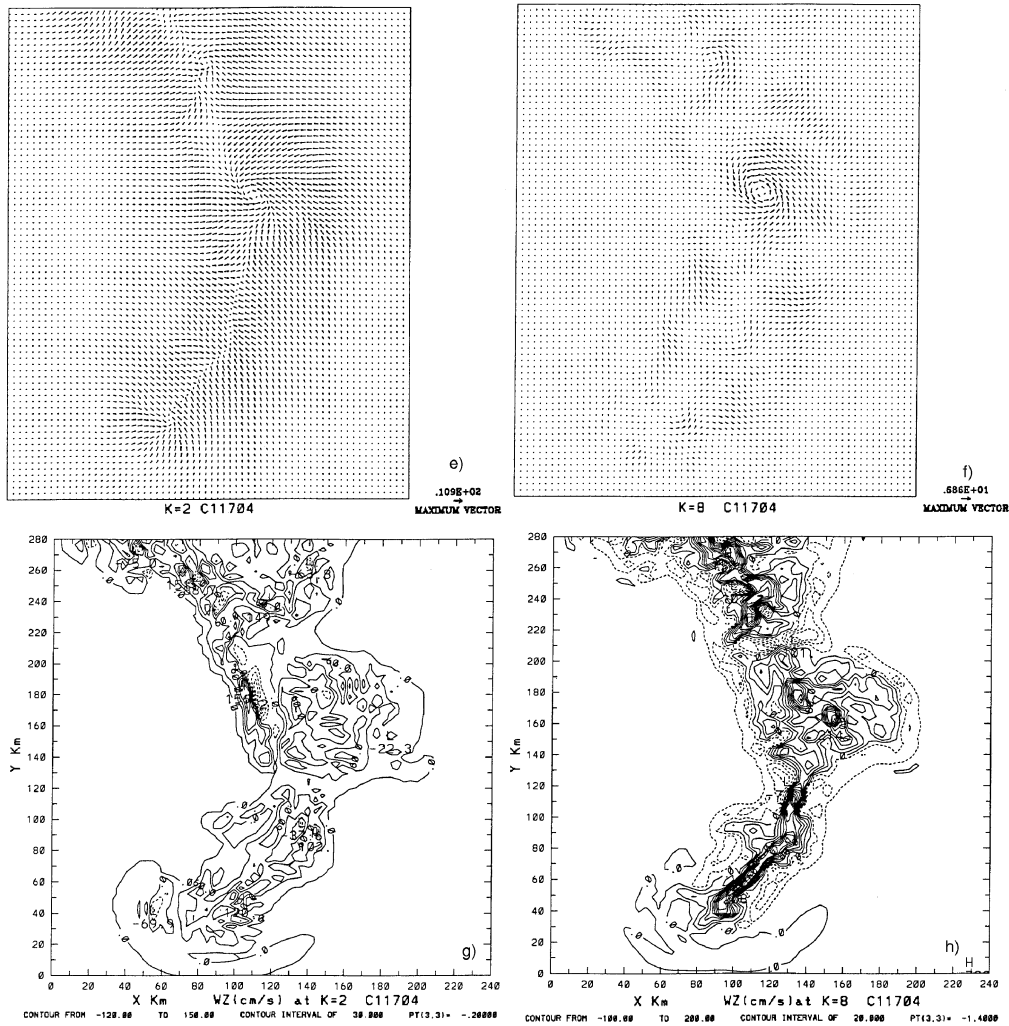


Fig. 2. - *Continued.* e) Horizontal wind field at $z = 100$ m; f) horizontal wind field at $z = 1600$ m; g) w -component of wind field at $z = 1600$ m; h) w -component of wind field at $z = 1600$ m.

TFMCs are forced by the heat fluxes (sensible and latent fluxes) and their vertical development and intensity depend on the season, *i.e.* on the solar radiation and heat budgets.

Soil humidity and landscape play an important role on the heat budget at the surface, as well as the atmospheric stability and the intensity of the synoptic circulation.

Three different situations have been studied, referring to three different seasons: summer, autumn and winter; however, we have studied the summer case in greater detail, since TFMCs are more pronounced during the hot season, and we analyzed the

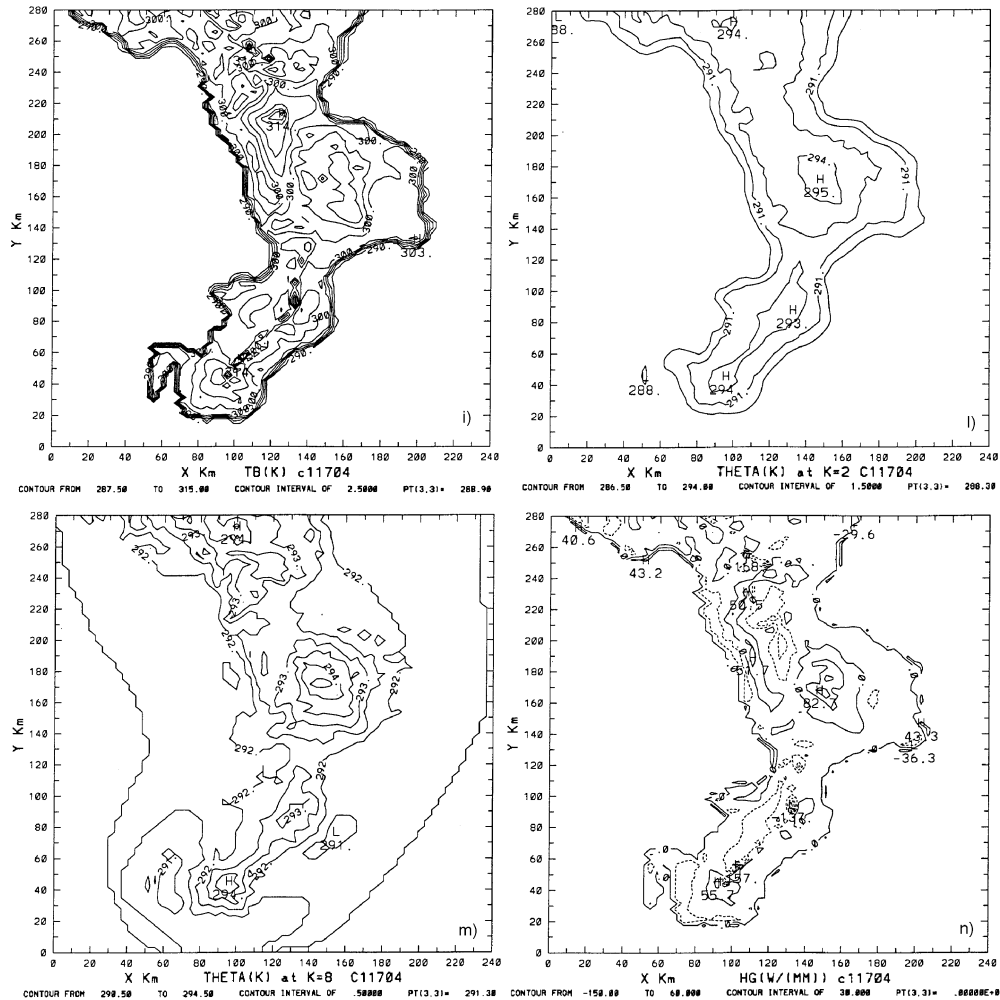


Fig. 2. - *Continued.* i) Surface temperature isolines; l) potential temperature isolines at $z = 100$ m; m) potential temperature isolines at $z = 1600$ m; n) sensible heat flux at the surface.

effects due to the following physical parameters: intensity of the large-scale flow represented by (u_g, v_g) , atmospheric stability, soil humidity.

The entire simulation domain extends for 300 km in the North-South direction and approximately 230 km in the East-West direction. The horizontal resolution is $\Delta x = \Delta y = 3.3$ km with 16 vertical layers not equally spaced, starting at the surface with the upper layer at 11 000 m, and including a dissipative layer above 5000 m. Due to the strong intensity of TFMCs and to their deep vertical extension, a second set of simulations have been performed, with the upper layer placed at 13 000 m, and the dissipative layer placed above 10 000 m. Only results relative to this second case are

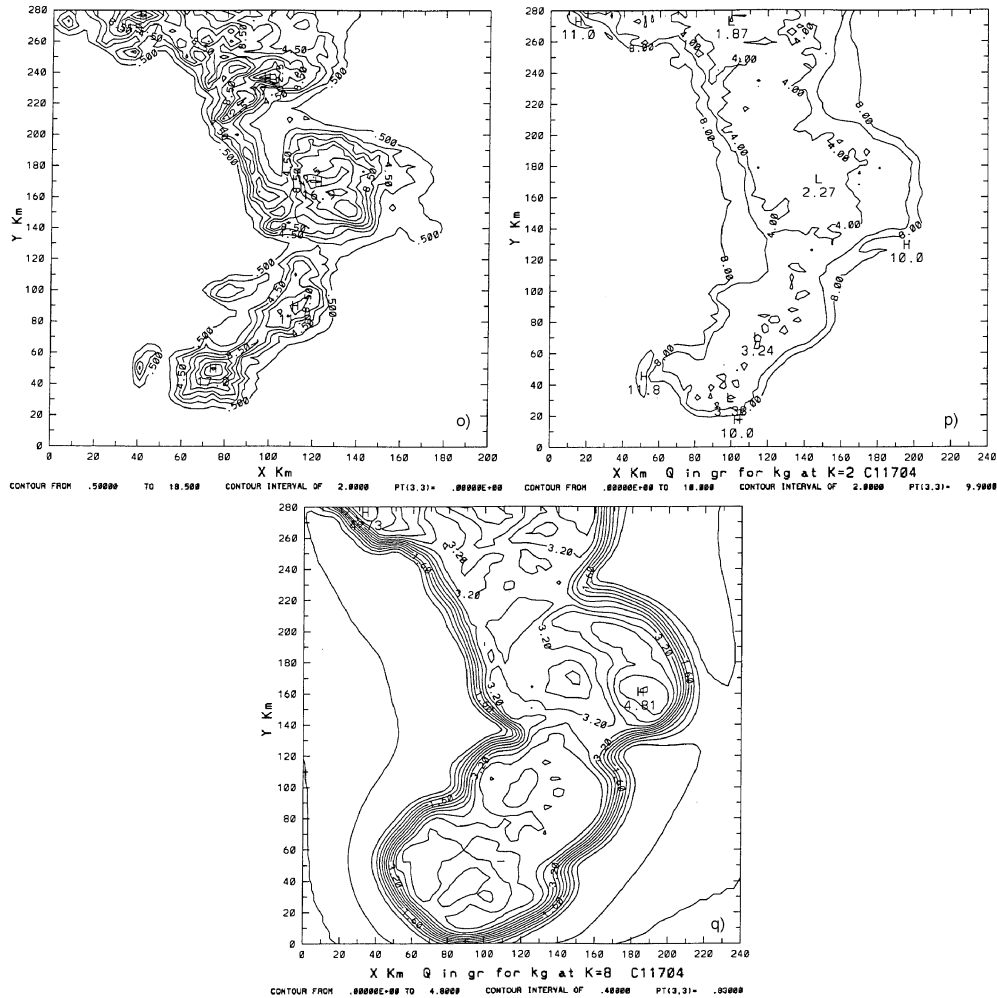


Fig. 2. - *Continued.* o) Latent heat flux at the surface; p) specific humidity isolines at $z = 100$ m; q) specific humidity isolines at $z = 1600$ m.

discussed in the present paper. In the vertical a terrain-following coordinate defined as [14]

$$z^* = s \frac{z - z_g}{s - z_g}$$

has been adopted, taking into account the topography of the region introduced as a lower boundary into the model.

The heat equation is numerically solved interactively with the equations for the long- and short-wave radiation balance and the latent and sensible heat equation in the

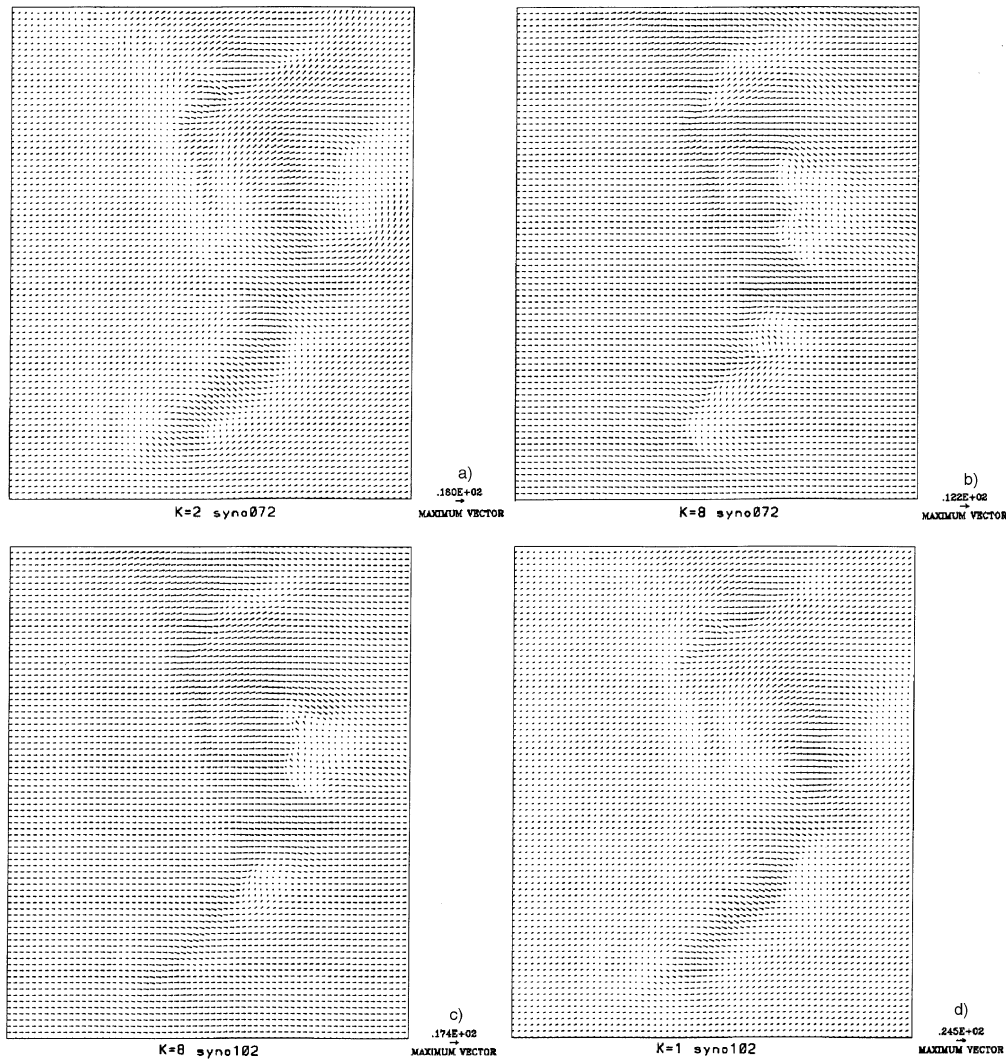


Fig. 3. - Summer case. Soil moisture = 0.05, conductivity = 3.9 cm/s, density = 1.45 kg/m³, specific heat = 0.35 cal/(cm³ K), surface temperature = 288 K, atmospheric stability = 2 K/km. a) horizontal wind field at $z = 100$ m, for mean synoptic wind $u_g = 7$ m/s; b) horizontal wind field at $z = 1600$ m, for mean synoptic wind $u_g = 7$ m/s; c) horizontal wind field at $z = 100$ m, for mean synoptic wind $u_g = 10$ m/s; d) horizontal wind field at $z = 1600$ m, for mean synoptic wind $u_g = 10$ m/s.

atmosphere. Furthermore, the initial humidity into the soil is given, and six soil levels have been used to take into account the vertical heat diffusion below the ground level, with a grid interval of 5 cm.

For all the simulations, the integration time is 12 hours, starting at 8:00 a.m. LST, and using a time step of 15 s.

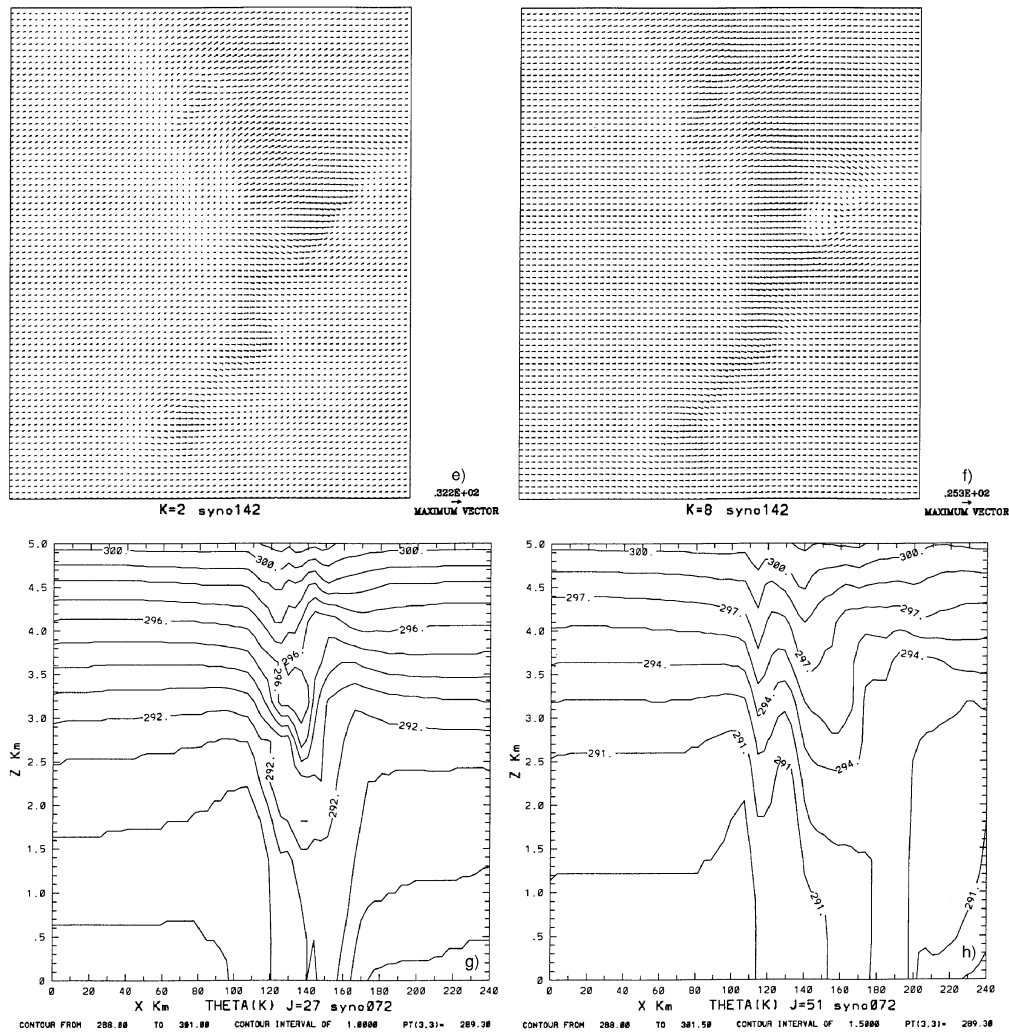


Fig. 3. - *Continued.* e) Horizontal wind field at $z = 100$ m, for mean synoptic wind $U_g = 14$ m/s; f) horizontal wind field at $z = 1600$ m, for mean synoptic wind $U_g = 14$ m/s; g) potential temperature vertical section ($j = 27$), for mean synoptic wind $U_g = 7$ m/s; h) potential temperature vertical section ($j = 51$), for mean synoptic wind $U_g = 7$ m/s.

4.1. Summer case. - Due to the presence of weak large-scale flows and strong insolation, the TFMCs are particularly intense during this season.

The two breeze systems: sea breeze and mountain breeze are superimposed due to the very steep mountain chain running all along the region and the narrowness of the region generating a low-altitude convergence and a divergence in the upper levels.

In fact, from the analysis of the complex meteorological phenomenology, an area of positive vorticity is present in the lower part of the troposphere and a negative one in

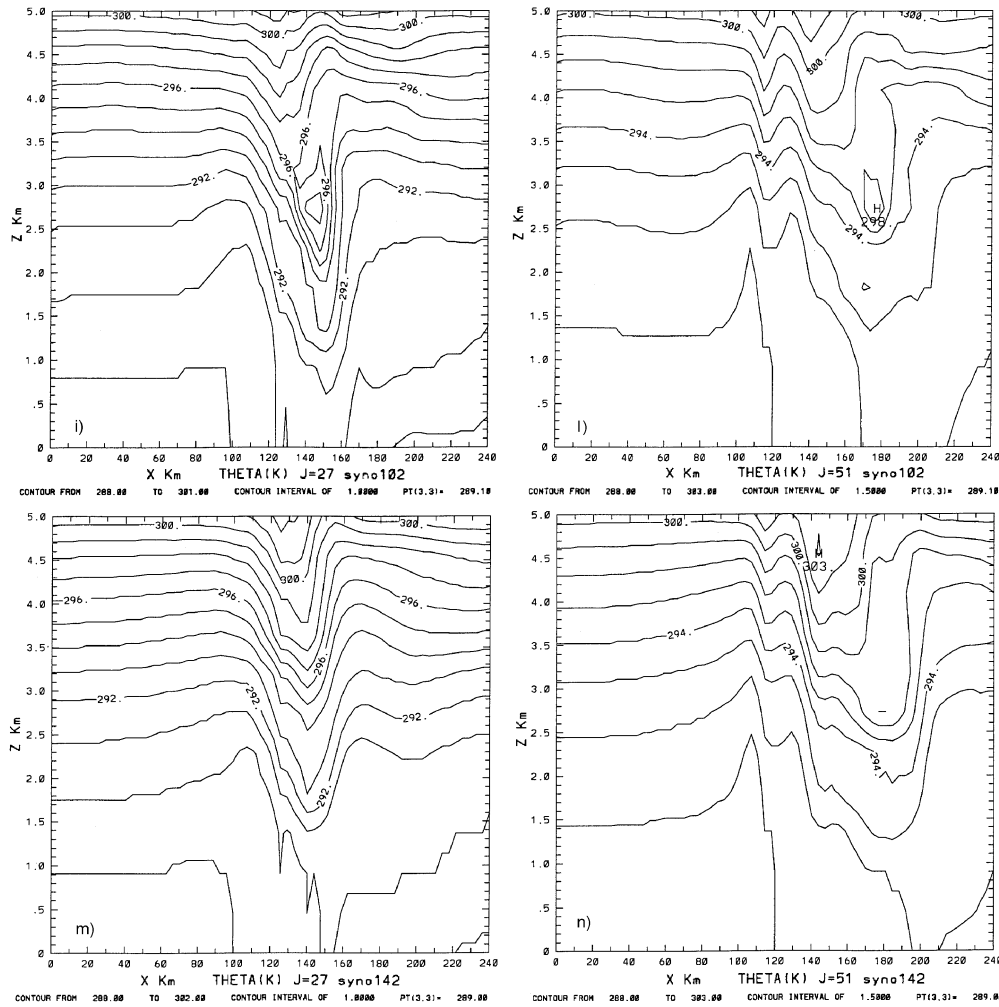


Fig. 3. - *Continued.* i) Potential temperature vertical section ($j = 27$), for mean synoptic wind $U_g = 10$ m/s; l) potential temperature vertical section ($j = 51$), for mean synoptic wind $U_g = 10$ m/s; m) potential temperature vertical section ($j = 27$), for mean synoptic wind $U_g = 14$ m/s; n) potential temperature vertical section ($j = 51$), for mean synoptic wind $U_g = 14$ m/s.

the higher layers with strong vertical velocity and storm clouds developing in the afternoon.

In order to study the summer case, several simulations with different soil moisture values and large-scale flow intensities have been performed.

41.1. Low-intensity synoptic flow, very dry soil, weakly stratified atmosphere. In this subsection we discuss results relative to 4:00 p.m. LST, *i.e.* after 8 hours of simulation. The large-scale flow is southerly with low wind intensity $U_g = 0$,

$v_g = 0.5$ m/s, and the soil rather dry with specific soil moisture = 0.05, conductivity = 3.9 cm/s, density = 1.45 kg/m³, specific heat = 0.35 cal/(cm³ K). The air temperature at the beginning of the simulation is $T = 288$ K and the atmospheric stability is 2 K/km.

Since the vertical development of the convection cell was limited by the height of the absorbing layer (5000 m) and of the top layer (10 000 m), in the following simulations the top layer height was placed at 13 000 m and the absorbing layer has

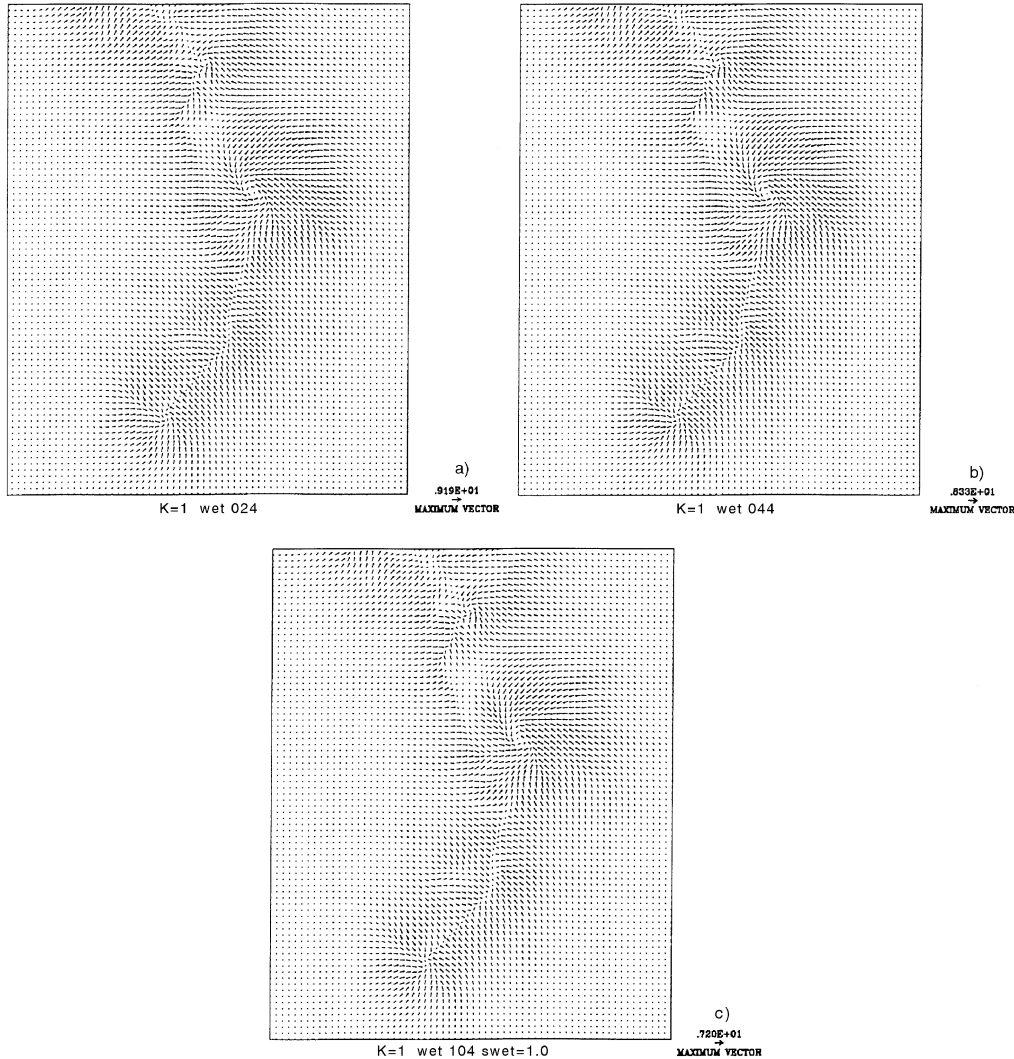


Fig. 4. - Summer case. Synoptic wind field = ($u_g = 0$; $v_g = 0.5$ m/s), conductivity = 3.9 cm/s, density = 1.45 kg/m³, specific heat = 0.35 cal/(cm³ K), surface temperature = 288 K, atmospheric stability = 2 K/km. a) horizontal wind field at $z = 50$ m, for soil moisture = 0.2; b) horizontal wind field at $z = 50$ m, for soil moisture = 0.4; c) horizontal wind field at $z = 50$ m, for soil moisture = 1.0.

been placed at 10 000 m. With these boundary conditions the TFMC can fully develop in the vertical, and reaches its mature state within the simulation time.

Figure 2a) and b) show the horizontal wind component isolines (u, v) at $z = 100$ m above the surface level (model level $k = 2$). Figure 2c), d) show u and v components at $z = 1600$ m (model level $k = 8$).

From fig. 2 we argue the presence of a strong convergence at low level (2a), b)), and a divergence at higher levels (fig. 2c), d)). The divergence is less intense than the convergence, with a divergent layer thicker than the convergent layer.

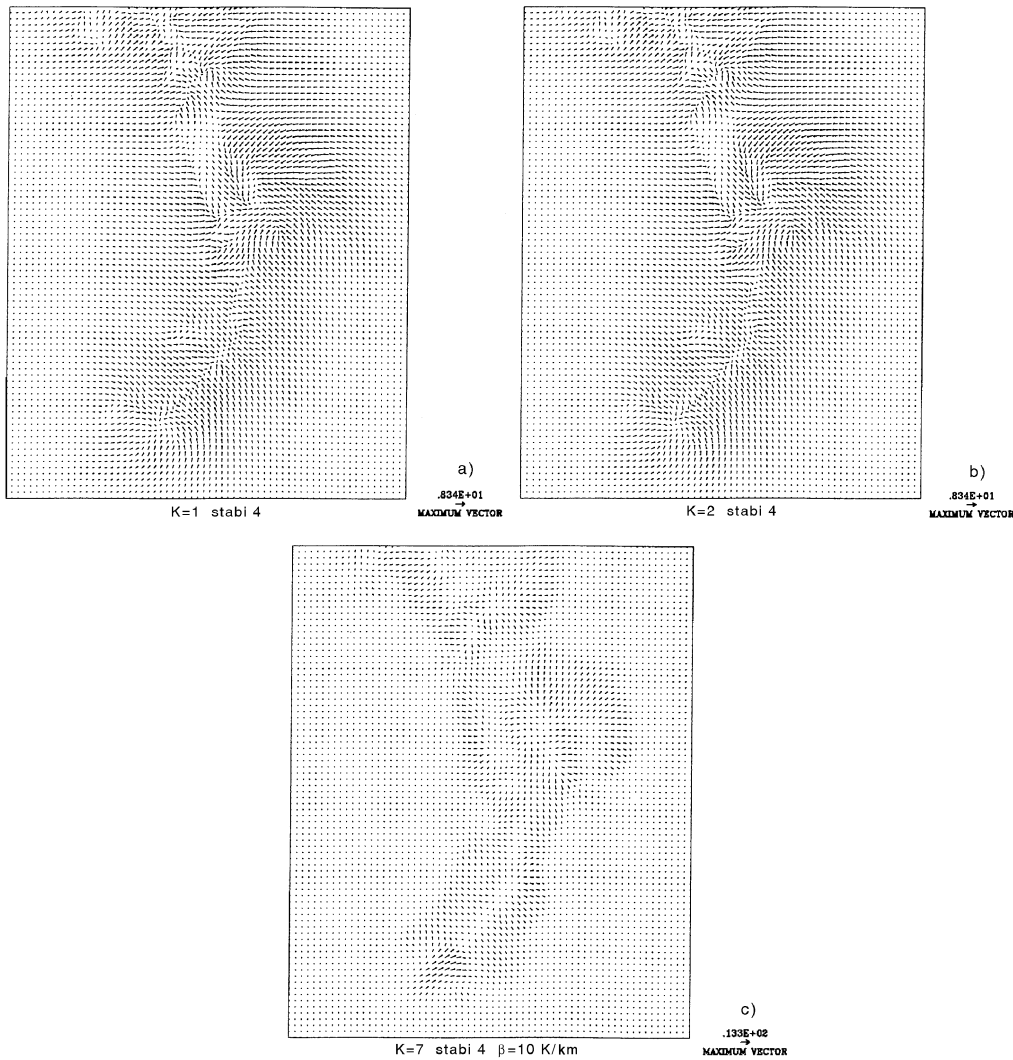


Fig. 5. - Summer case. Synoptic wind field = ($u_g = 0$; $v_g = 0.5$ m/s), soil moisture = 0.05, conductivity = 3.9 cm/s, density = 1.45 kg/m³, specific heat = 0.35 cal/(cm³ K), surface temperature = 288 K. a) Horizontal wind field at $z = 50$ m, for potential temperature gradient = 10 K/km; b) horizontal wind field at $z = 100$ m, for potential temperature gradient = 10 K/km; c) horizontal wind field at $z = 1100$ m, for potential temperature gradient = 10 K/km.

The same situation is present if we consider the wind vector: *i.e.* we have an intense convergence at $z = 100$ m (fig. 2e)), with a cyclonic rotation of the flow such that the orography contours of the region are clearly visible.

However, at higher levels, $z = 1600$ m (fig. 2f)), a weak cyclonic circulation is present directly above the Appennines, while the flow is anticyclonic far from the mountains in the downwelling region.

Since the vertical velocity is given by the vertical integral of the horizontal divergence, and the divergence is positive, directly above the mountain range, even at

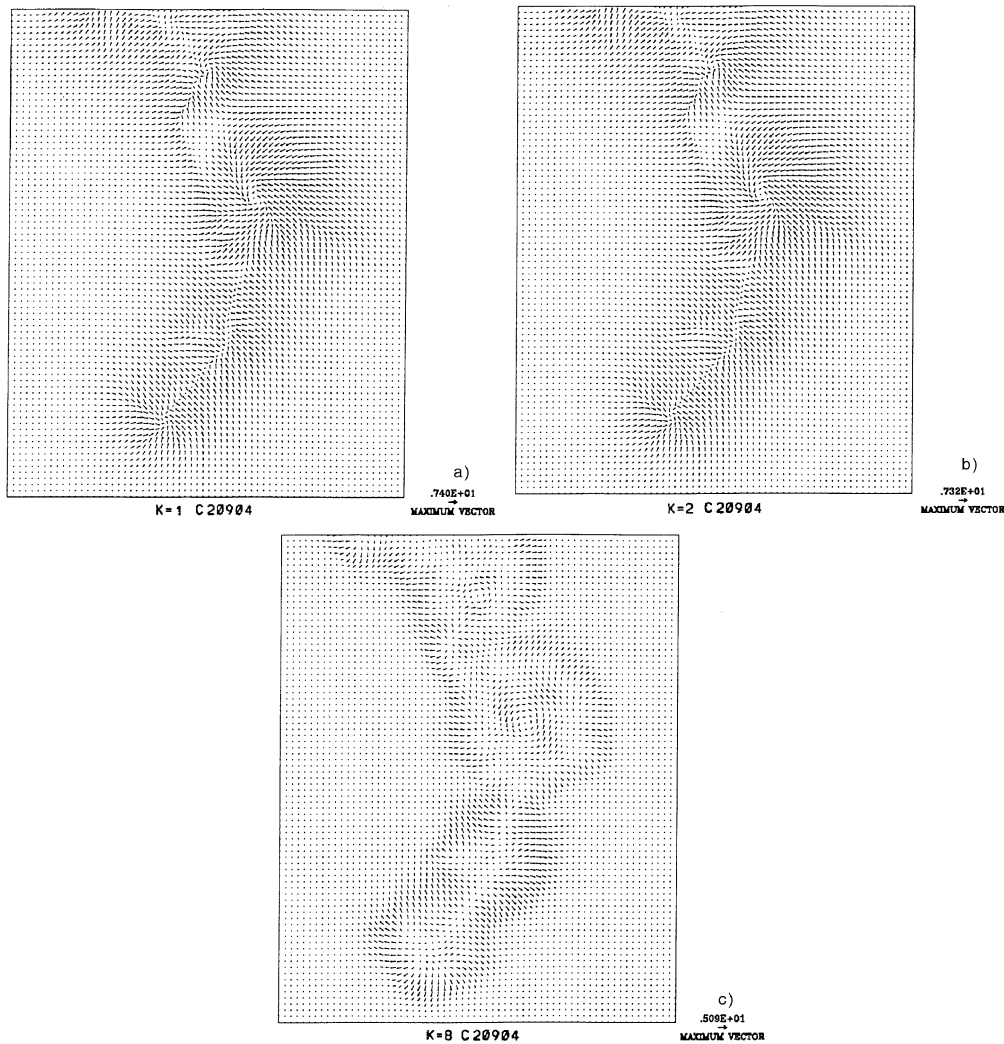


Fig. 6. - Autumn case. Synoptic wind field = ($u_g = 0$; $v_g = 0.5$ m/s), soil moisture = 0.05, conductivity = 3.9 cm/s, density = 1.45 kg/m³, specific heat = 0.35 cal/(cm³ K), surface temperature = 288 K, atmospheric stability = 2 K/km. a) horizontal wind field at $z = 50$ m; b) horizontal wind field at $z = 100$ m; c) horizontal wind field at $z = 1600$ m.

higher levels, it follows that the vertical velocity is positive and an intense convective activity is present at that level (fig. 2g, h)). In addition, the vertical velocity isolines show that w is more intense in the upper layer than in the lower layer, and narrow convective aisles are present, extending from the mountain peaks up to the troposphere, while the vertical velocity is negative in the upper layers above flat areas, coastlines, sea.

The potential temperature field at different altitudes above the surface (0 m, 100 m, 1600 m) is shown in fig. 2i), l), m). While the low level field 2i) shows clearly the strong

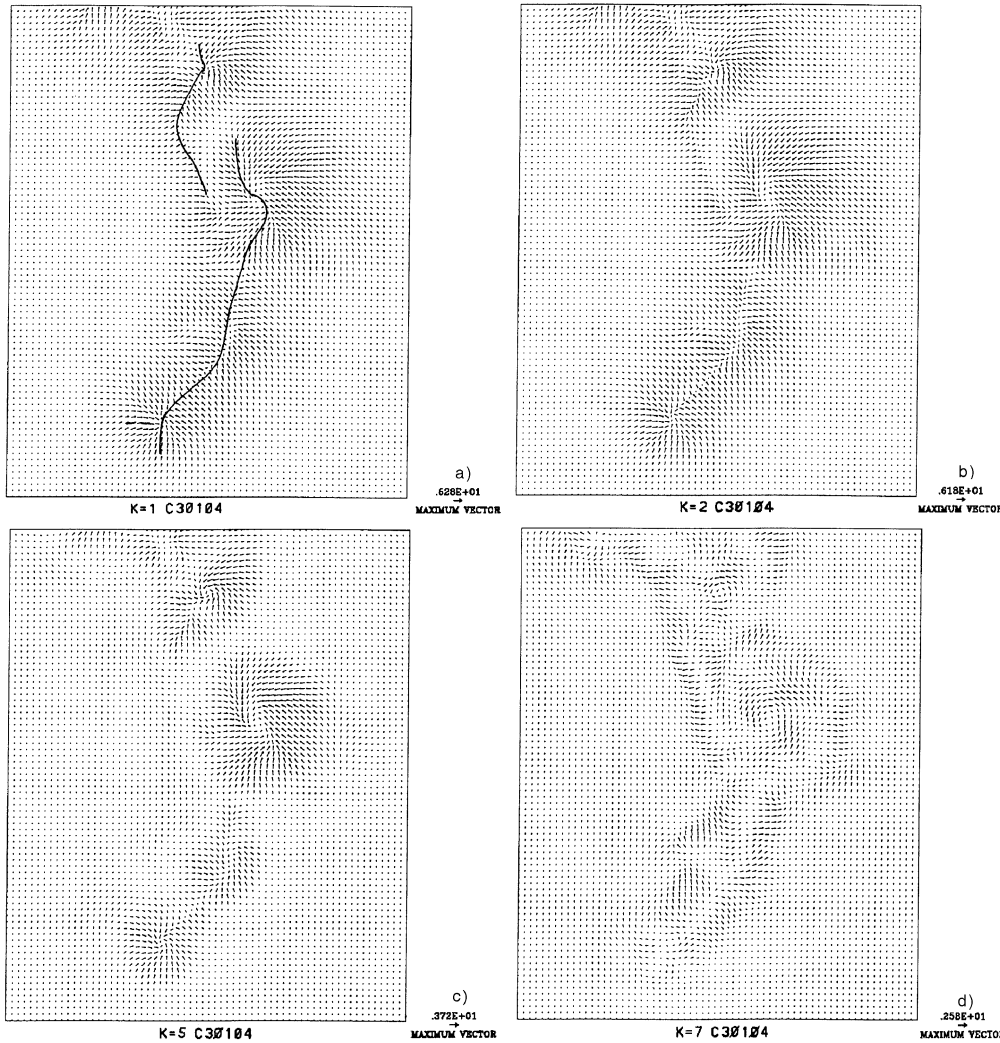


Fig. 7. - Winter case. Synoptic wind field = $(U_g = 0; V_g = 0.5 \text{ m/s})$, soil moisture = 0.05, conductivity = 3.9 cm/s, density = 1.45 kg/m³, specific heat = 0.35 cal/(cm³ K), surface temperature = 288 K, atmospheric stability = 2 K/km. a) horizontal wind field at $z=50 \text{ m}$; b) horizontal wind field at $z=100 \text{ m}$; c) horizontal wind field at $z=600 \text{ m}$; d) horizontal wind field at $z=1100 \text{ m}$.

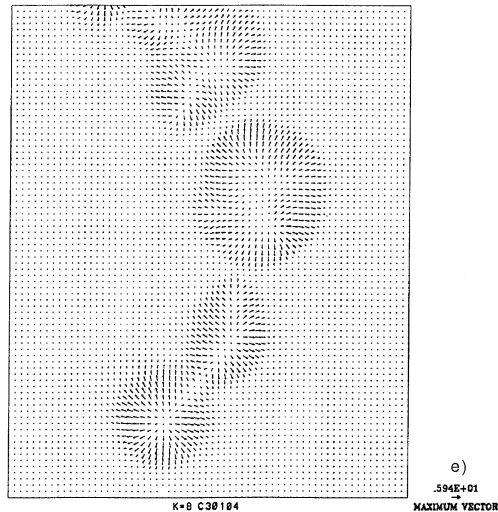


Fig. 7. - *Continued.* e) Horizontal wind field at $z = 1600$ m.

horizontal gradient due to the presence of the warm sea, the isotherms at $z = 100$ m clearly delineate the contour of the region, and the location of the highest mountains is clearly marked by the presence of the warmer isolines showing, as expected, the effect of the mountain as heat source.

The sensible heat flux and the latent heat flux are plotted in fig. 2n) and o), respectively. However, humidity field analysis is a better tracer when studying the intensity and the development of convective clouds (fig. 2p), q).

4.1.2. Non-zero synoptic flow, very dry soil, weakly stratified atmosphere.

In this case we studied the influence of a synoptic flow on the TFMCS. We analyzed three different situations relatively to three different values of the intensity of the large-scale westerly flow: $u_g = 7$ m/s, $u_g = 10$ m/s, $u_g = 14$ m/s. As in the previous case, the soil is rather dry with specific soil moisture = 0.05, conductivity = 3.9 cm/s, density = 1.45 kg/m³, specific heat = 0.35 cal/(cm³ K). The initial air temperature at the surface is $T = 288$ K and the atmospheric stability is assumed to be 2 K/km.

In fig. 3 we present results after 4 hours of simulation, *i.e.* at 12:00 p.m. LST, at two different levels, 100 m and 1600 m, for different values of synoptic wind intensity: 7 m/s (fig. 3a), b)), 10 m/s (fig. 3c), d)), 14 m/s (fig. 3e), f)).

Comparing the wind field in the three different cases, we can see that the TFMCS are less intense, and advected downwind, assuming a more asymmetric shape, when the synoptic wind intensity increases.

Mesoscale circulation switches from a thermally forced flow to a synoptic flow orographically perturbed with generation of gravity waves, as shown in East-West cross-sections of potential temperature field (fig. 3g), h), i), l), m), n)).

4.1.3. Influence of soil humidity on TFMCS. In this case we assume that the synoptic flow is almost zero and the atmospheric stability is almost neutral, and we

study how changes in soil humidity can affect TFMCs. We assume four different values of soil humidity: 0.05, 0.2, 0.4, 1. Since the latent heat of water has a very high value, soil specific humidity strongly affects latent and sensible heat fluxes, and, for increasing soil humidity, latent heat flux increases, while sensible heat flux, which forces the TFMCs formation, decreases.

However, the phenomenon is rather complex. In fact, increasing the latent heat flux out of the soil, the air specific humidity increases, increasing also the possibility of water condensation and subsequent heat formation, whenever the Lifting

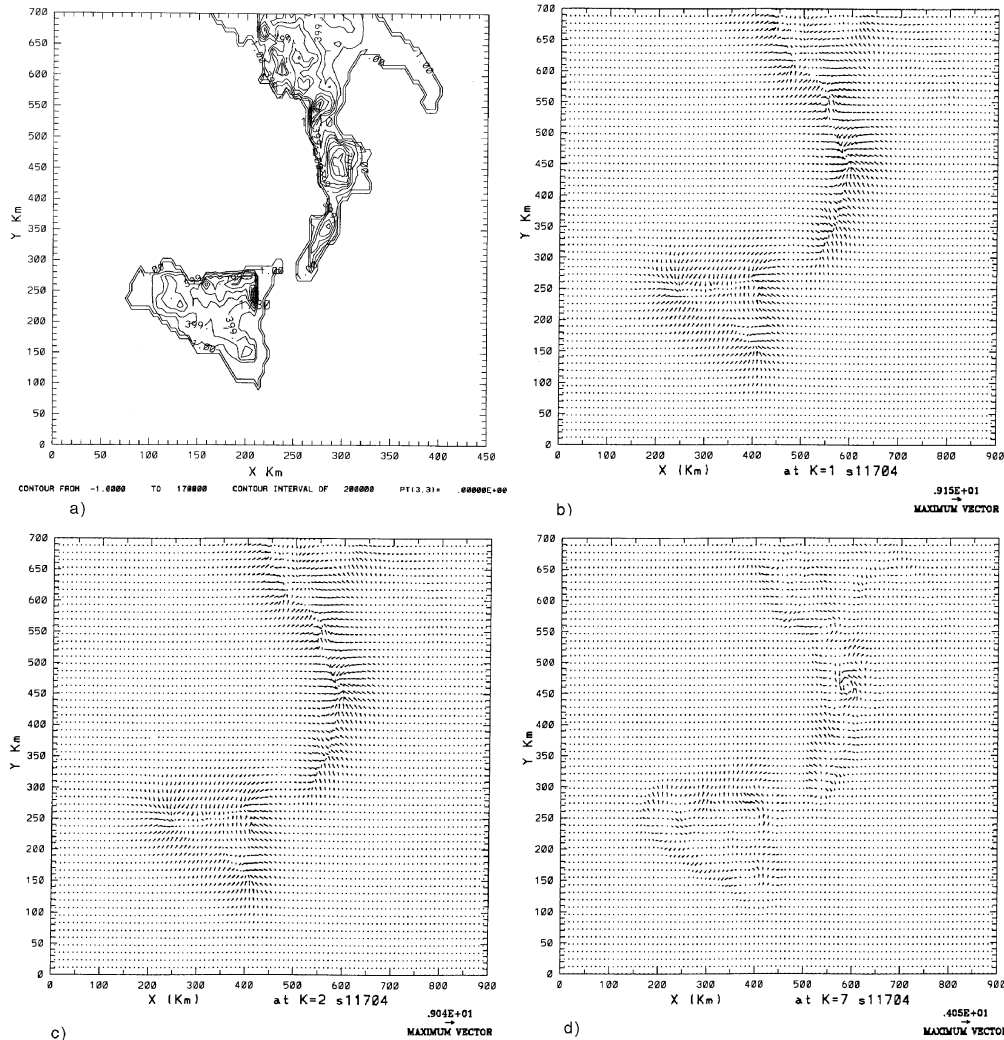


Fig. 8. - Summer case. Soil moisture = 0.05, conductivity = 3.9 cm/s, density = 1.45 kg/m³, specific heat = 0.35 cal/(cm³ K), surface temperature = 288 K, atmospheric stability = 2 K/km. a) Orography of the Calabria and Sicily Region; b) horizontal wind field at z = 50 m, for mean synoptic wind $u_g = 7$ m/s; c) horizontal wind field at z = 100 m, for mean synoptic wind $u_g = 7$ m/s; d) horizontal wind field at z = 1100 m, for mean synoptic wind $u_g = 7$ m/s.

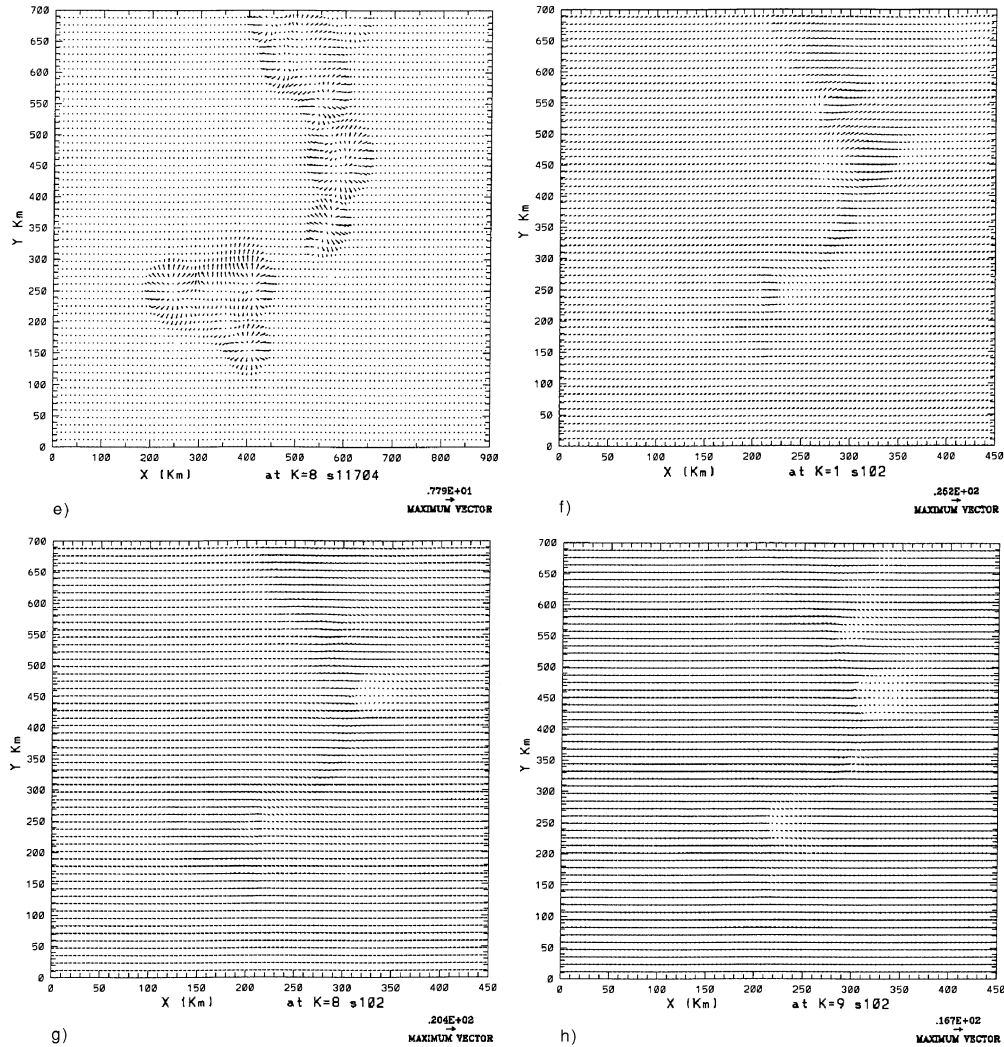


Fig. 8. - *Continued.* e) Horizontal wind field at $z = 1600$ m, for mean synoptic wind $U_g = 7$ m/s; f) horizontal wind field at $z = 50$ m, for mean synoptic wind $U_g = 10$ m/s; g) horizontal wind field at $z = 1600$ m, for mean synoptic wind $U_g = 10$ m/s; h) horizontal wind field at $z = 2400$ m, for mean synoptic wind $U_g = 10$ m/s.

Condensation Level (LCL) is reached, LCL being the level at which water vapor condenses.

We discussed the first case with dry soil (soil moisture = 0.05) in a previous paragraph (fig. 2), and now we analyze the wind field at $z = 50$ m, for increasing soil humidity: the TFMCs intensity decreases for increasing soil humidity (fig. 4). The apparent similarity between the different cases is only due to the graphic representation of the phenomenon.

4.1.4. Influence of atmospheric stability on TFMCs. In this case we simulated the effects due to a stable atmosphere with a vertical potential temperature gradient equal to 10 K/km, for low synoptic wind intensity.

In fig. 5a)-c) we show wind field at $z = 50$ m, 100 m, 1100 m, respectively. TFMCs flow follows the orography contours, in the presence of stable atmospheric conditions, and the atmospheric circulation is less intense and penetrating in the upper layer, due to the less intense fluxes of sensible heat.

4.2. *Autumn case.* – This case refers to the month of October, and the simulation is for a very dry soil, stable atmosphere and weak synoptic flow. TFMCs are not as intense as in summer, since the solar radiation reaching the surface is less intense than in the previous case.

Mesoscale atmospheric flow follows the orography (fig. 6a), b)) in the lower layer, as in summer, and the perturbation in the upper layer is weaker; however, TFMCs above the mountain peaks, at $z = 1600$ m, are still present (fig. 6c)).

4.3. *Winter case.* – Wintertime TFMCs are very similar to TFMCs in autumn, but they are less strong. At the surface (fig. 7a)) the convergence of the flow is quite strong and the flow runs along the highest orography isolines.

The flow in the upper layers, similar in its general pattern to the autumn case, is shown in fig. 7b)-e).

4.4. *Summer case: the influence of Sicily Island.* – Last, we analyzed the effects due to the presence of Sicily Island during summer, for high values of solar radiation and weak and strong synoptic wind. In the first case, the influence of the Island is evident in the deformation of the flow in the southern part of Calabria, while in the second case it varies depending on synoptic wind intensity and direction.

However, a more detailed study is necessary to better understand the more complex flow circulation.

For a grid resolution of $\Delta x = \Delta y = 3.3$ km, and a synoptic westerly wind velocity $U_g = 10$ m/s, Sicily Island effects are more evident and effective (fig. 8f)-h)) than for a calm situation (fig. 8b)-d)).

5. – Conclusions

The present study investigated the structure and formation of thermally forced mesoscale circulation under calm and initially clear-sky synoptic conditions, over Calabria, Italy, and the seasonal variation of TFMCs; the impact of the soil moisture availability, of the background atmospheric thermal stability and of the synoptic flow intensities on TFMCs structures using a 3D numerical mesoscale model.

The main conclusions are as follows:

- The thermally forced mesoscale circulation over Calabria, a mountaineous region surrounded by the sea on the West, South and East sides, is likely to be more

pronounced than that over most of the midlatitude area, by the interactions between sea breeze circulation and upslope flow circulation. The daytime upslope flow circulation is strong because of the steepness of the Apennines, and the thermally induced mesoscale circulations are supported by sea breezes. Therefore, the updraft, in the front of the intensified circulation over the convergent zone, is very strong. Since the West-East spatial scale of Calabria is of the order of 100 km, the intensified head-on moving upslope circulation would meet at or after noon. The collision will result in stronger upward motion. The humid air evaporated from the sea will be organized by the TFMCS and transferred to the convergent zones where it moves upward to form convective clouds. The above processes play a fundamental role in local climate and are responsible for thunderstorms occurring in winter season in Calabria.

- The impact of the thermal stability of the environment on flow field in lower layers of PBL is not very strong. However, the flow depth and the structures of both the temperature and the humidity fields are affected by its changes. The flow depth decreases and the horizontal gradients of potential temperature and specific humidity increase when the background stability increases.

- Increasing the soil moisture available will decrease the amplitude of the thermally forced mesoscale circulation, and the impact of these parameters has nonlinear effects on TFMCS evolution.

- The simulation results and scaling analysis suggest that the TFMCS are proportional to the square root of the surface sensible heat flux. The sensible heat flux is proportional to the intensity of the incoming solar radiation flux and decreases when the soil moisture availability increases. Its impact on sensible heat flux is rather complex and needs further investigation.

- By the action of synoptic flow, thermally induced mesoscale flow circulations are shifted downwind, the movement depending on the intensity of the synoptic flow itself. TFMCS structure changes because of the interaction between the synoptic flow and the topography and because of the interaction between synoptic flow with the TFMCS themselves.

* * *

This research has been financed by CNR-PP.SS. "MAP" and "Ambiente e Territorio".

REFERENCES

- [1] PIELKE R. A., COTTON W. R., WALKO R. L., TREMBACK C. J., LYONS W. A., GRASSO L. D., NICHOLLS M. E., MORAN M. D., WESLEY D. A., LEE T. J. and COPELAND J. H., *Meteorol. Atmos. Phys.*, **49** (1992) 69.
- [2] MAHRER Y. and PIELKE R. A., *Contr. Atmos. Phys.*, **50** (1977) 98.
- [3] METEOROLOGICAL OFFICE, *Weather in the Mediterranean*, Vols. **I, II**, 2nd edition (General Meteorology H. M. Stat. Office, London) 1962.
- [4] COLACINO M., in *Winds and Currents of the Mediterranean Basin*, edited by H. CHARNOCK, *Repts. Meteor. Oceanogr.*, no. **40** (Harvard University) 1992.

- [5] COLACINO M., CONTE M. and PIERVITALI E., *Elementi di Climatologia della Calabria, Collana P.S. "Clima, Ambiente e Territorio nel Mezzogiorno"*, edited by A. GUERRINI (CNR, Roma) 1997.
- [6] PIELKE R. A., *Mon. Weath. Rev.*, **102** (1974) 115.
- [7] TRIPOLI G. J. and COTTON W. R., *J. Rech. Atmos.*, **16** (1982) 185.
- [8] TREMBACK C. J., POWELL J., COTTON W. R. and PIELKE R. A., *Mon. Weath. Rev.*, **115** (1985) 540.
- [9] KALLOS G., *Environ. Software*, **4** (1989) 117.
- [10] SEGAL M., MCNIDER R. T., PIELKE R. A. and MCDUGAL D. S., *Atmos. Environ.*, **16** (1982) 1381.
- [11] SEGAL M., PIELKE R. A., ARRIFF R. W., MORAN M. D., YU C. H. and HENDERSON D., *Atmos. Environ.*, **22** (1988) 1319.
- [12] PIELKE R. A. and ULIASZ M., *Atmos. Environ.*, **32** (1998) 1455.
- [13] MAHRER Y. and PIELKE R. A., *Mon. Weath. Rev.*, **106** (1978) 818.
- [14] PIELKE R. A. and MARTIN C. L., *J. Atmos. Sci.*, **38** (1981) 1707.